applied sciences

MDPI

Article

Tuned Mass Damper Design for Slender Masonry Structures: A Framework for Linear and Nonlinear Analysis

Marco Zucca [1,*], Nicola Longarini [1], Marco Simoncelli [1] and Aly Mousaad Aly [2]

[1] Department of Architecture, Built Environment, and Construction Engineering, Politecnico di Milano, 20133 Milan, Italy; nicola.longarini@polimi.it (N.L.); marco.simoncelli@polimi.it (M.S.)
[2] Department of Civil And Environmental Engineering, Louisiana State University, Baton Rouge, LA 70803, USA; aly@lsu.edu
* Correspondence: marco.zucca@polimi.it

Abstract: The paper presents a proposed framework to optimize the tuned mass damper (TMD) design, useful for seismic improvement of slender masonry structures. A historical masonry chimney located in northern Italy was considered to illustrate the proposed TMD design procedure and to evaluate the seismic performance of the system. The optimization process was subdivided into two fundamental phases. In the first phase, the main TMD parameters were defined starting from the dynamic behavior of the chimney by finite element modeling (FEM). A series of linear time-history analyses were carried out to point out the structural improvements in terms of top displacement, base shear, and bending moment. In the second phase, masonry's nonlinear behavior was considered, and a fiber model of the chimney was implemented. Pushover analyses were performed to obtain the capacity curve of the structure and to evaluate the performance of the TMD. The results of the linear and nonlinear analysis reveal the effectiveness of the proposed TMD design procedure for slender masonry structures.

Keywords: masonry structures; seismic assessment; TMD; pushover analysis; nonlinear analysis

Citation: Zucca, M.; Longarini, N.; Simoncelli, M.; Aly, A.M. Tuned Mass Damper Design for Slender Masonry Structures: A Framework for Linear and Non-Linear Analysis. *Appl. Sci.* **2021**, *11*, 3425. https://doi.org/10.3390/app11083425

Academic Editors: Marek Krawczuk and Elsa Caetano

Received: 2 March 2021
Accepted: 9 April 2021
Published: 11 April 2021

1. Introduction

Many important historical constructions are built in high seismicity areas and nowadays require interventions to improve their resilience. Considering the Italian historical heritage, several buildings that were originally designed to resist only gravity loads suffered serious damages during recent strong earthquakes, such as L'Aquila (2009) [1–5], Emilia-Romagna (2012) [6,7], Amatrice (2016) [8,9], and Ischia (2017) [10,11]. Several researchers have proposed different techniques to improve the seismic behavior of historical buildings, for example, by the application of noninvasive and reversible systems [12–17]. Removeable systems are often required to restore the original structure. Therefore, it is possible to improve the structure's seismic response by invasive modification of the original structure (solution 1) or by applying an auxiliary and reversible system that changes its dynamic response (solution 2).

To improve the seismic behavior of slender masonry constructions, such as chimneys or towers, the use of steel reinforcements rings attached to the primary structure by steel rebars is commonly adopted (solution 1) [18]. In other cases, an inner spiral reinforcement is applied, as shown in Figure 1. For these slender constructions, structural improvements are necessary to overcome the dynamic effects caused by wind and/or seismic actions.

(**a**) (**b**)

Figure 1. The use of steel reinforcements rings to improve the seismic behavior of slender masonry constructions (invasive modification of the original structure (solution 1). (**a**) Outer reinforcement, and (**b**) inner reinforcement.

Solution 2 is largely used in slender concrete [19–21] and steel [22–24] constructions. Possible examples of this solution are the chimney presented in [25] and the "Arquata Scrivia chimney" (Figure 2). In both cases, the used system was a tuned mass damper (TMD). TMDs have shown their effectiveness and robustness as vibration countermeasures tall and slender constructions, such as high-rise buildings and wind turbines . To design a TMD, different criteria should be considered, taking into account the possible distinct interactions of wind and earthquake with the structure. The application of the TMD on reinforced concrete and steel slender structures is deeply investigated [26–30]. However, there are no common examples of the application of a TMD on slender historical masonry construction. In the following, the criteria to design and optimize a TMD for a masonry slender structure are pointed out, considering, as an example, the case of a chimney part of a historical hydraulic plant. For this chimney, the owner requested a removable system to improve its seismic behavior. Furthermore, an appreciable combination of the TMD steel support structure with the existing masonry one was also needed. Figure 3 shows the first configuration with the TMD located at the top of the chimney. Another possible configuration of the TMD steel support structure is demonstrated in Figure 4 (second configuration).

Figure 2. Arquata Scrivia chimney (AL, Italy). An example of applying an auxiliary and reversible system that changes its response under dynamic loads (solution 2).

(**a**)

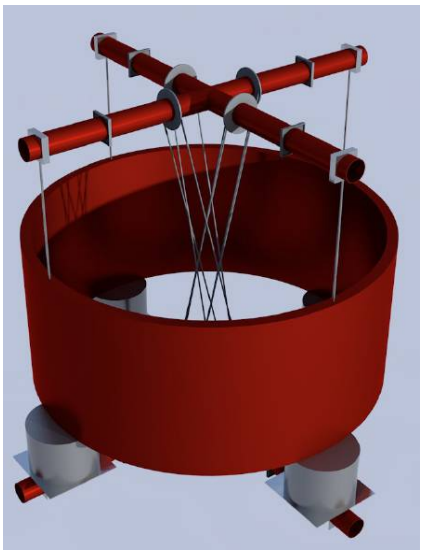

(**b**)

(**c**)

Figure 3. A 3D render of the real, tuned mass damper (TMD) design for a masonry slender structure proposed to the Italian Cultural Heritage. (**a**) The proposed first configuration with the TMD located near the top of the chimney, (**b**) steel TMD in detail, and (**c**) view of the historical hydraulic plant (Italy).

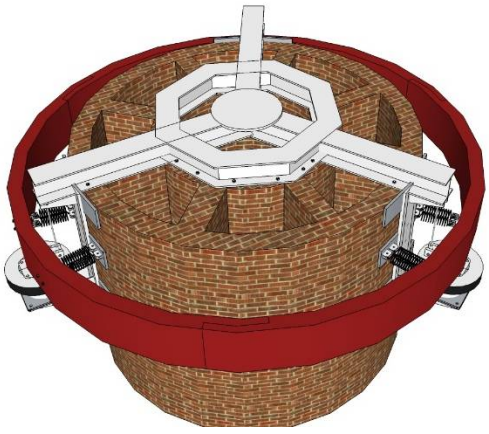

(**a**)

(**b**)

Figure 4. Proposed second configuration with the TMD located at the top of the chimney: (**a**) detail of the TMD support steel structure, and (**b**) a view of the damping devices.

In approaching a historical construction, two preliminary activities are required: (i) the geometric survey and (ii) the dynamic tests [31]. With the geometric survey, it is possible to determine the geometric characteristics of the main structural elements, which for the chimney under study are the inner and the outer skin, the 8 meridians, and 11 parallels. It should be highlighted that the chimney is characterized by a height equal to 50 m, considering the presence of a 10 m height basement, which presents a stiffness significantly greater than that of the chimney (Figure 5). For this reason, to define the dynamic behavior of the historical chimney, only the upper slender part is considered.

The chimney presents the inner and outer skins from the base to 26.50 m in height. The outer skin is characterized by a tapered section with a diameter ranging between 3.70 m at the base to 2.62 m at the height of 26.50 m. Above the quote of 26.50 m, the chimney has only one skin (the external one) with different thicknesses: 0.51 m from 26.50 m to 28.00 m, 0.37 m from 28.00 m to 28.90 m, 0.33 m from 28.90 m to 29.23 m, and 0.28 m up to the top.

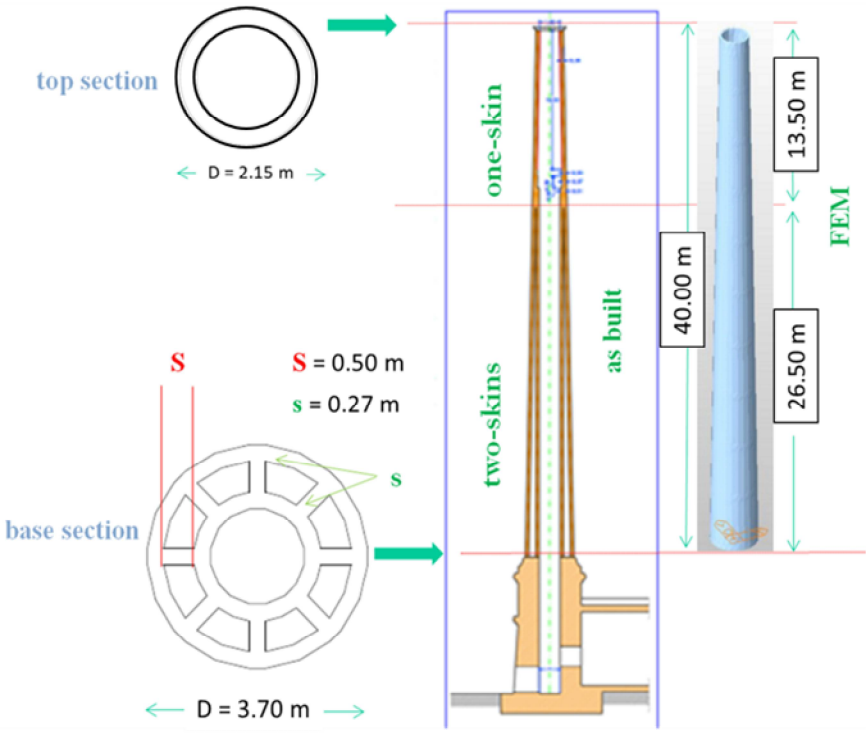

Figure 5. The historical masonry chimney under study.

Regarding the mechanical property of the masonry, flat jacks tests in different positions of the chimney were executed to evaluate the compression resistance (f_d) and Young's modulus (E_d) [32]. After the test it was obtained a masonry compressive strength, f_d = 4.96 MPa, and a value of Young's modulus E_d = 7150 MPa. As deeply discussed in [33,34], it is necessary to reduce the value of the compressive strength obtained from the in situ tests by the following:

$$f_{d,red} = (f_d/c_1) \cdot c_2 = 3.55 \text{ MPa}, \quad (1)$$

where $c_1 = 1.2$ is a coefficient that considers the number of tests carried out, and $c_2 = 0.86$ is a coefficient that considers the geometrical slenderness of the structure and the eccentricity of the vertical loads acting on the considered structure.

2. TMD Optimization Framework

The main steps of the optimization procedure of the TMD design are summarized in Figure 6. The proposed procedure is based on two main steps. In the first step, the

dynamic behavior of the analyzed structure is obtained through the implementation of a simplified finite element model to calculate the fundamental characteristics of the TMD after an optimization process performed by the execution of linear time-history analyses. Defined the TMD properties, expressed in terms of mass, equivalent stiffness, and equivalent damping; in the second step, the operating limit of the optimized TMD is evaluated considering a fiber model where the nonlinear behavior of the masonry is considered.

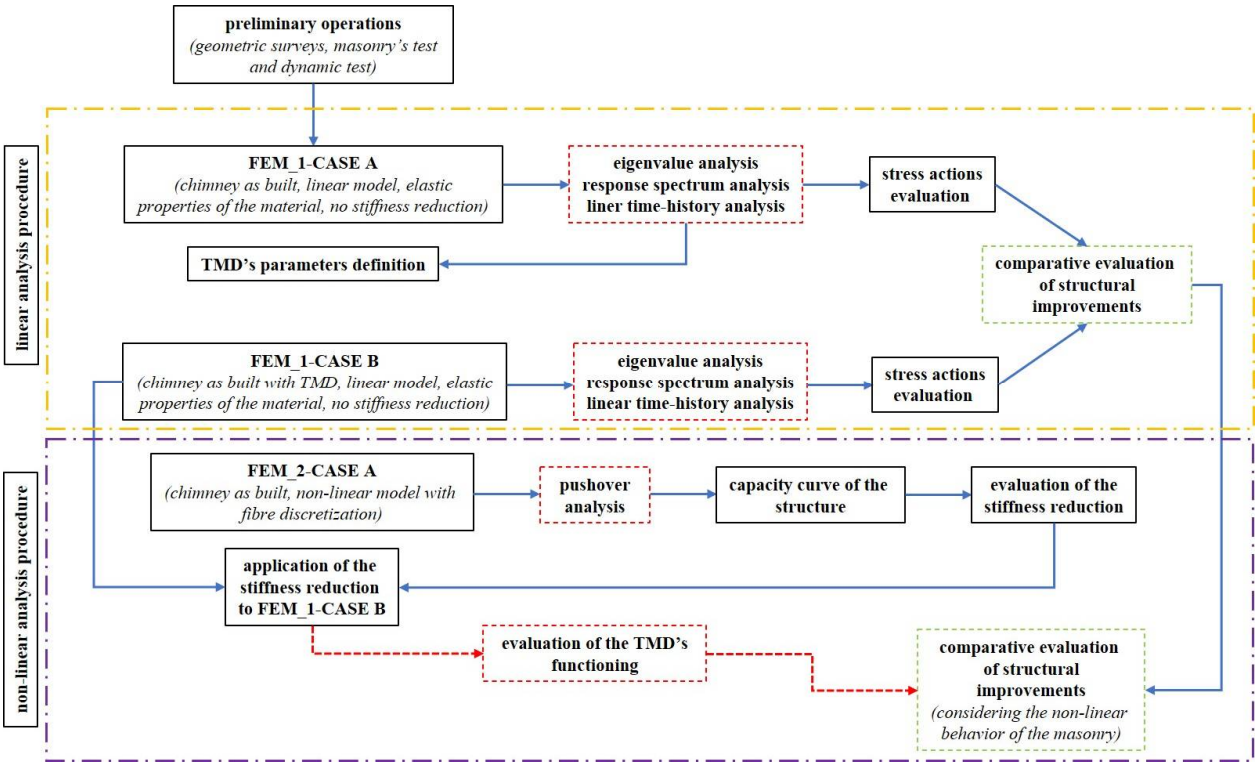

Figure 6. Flow diagram of the proposed optimization procedure.

Knowing the geometry and the mechanical characteristics of the masonry, a first linear elastic finite element model (FEM_1—CASE A) of the chimney was implemented through Midas GEN software [35], where the structure is schematized only with tapered beam elements (Figure 7) in the typical cantilever configuration with a fully constrained boundary condition at the base. An eigenvalue analysis was executed by updating the stiffness value of the different sections that characterized the chimney under study to reproduce the experimental results obtained from the dynamic test [36] performed by a specialized Italian company in 2015 (Table 1). Four three-axis MEMS accelerometers have (www.microseismic.com, accessed in 2021) were located along the tower in two different configurations: Config. 1, a distance of 30 m, 38 m, 44 m and 50 m from the base level; Config. 2, a distance of 10.5 m, 20 m, 30 m and 38 m from the base. The reference point of all the measures was the accelerometer located at 38 m of height. The sampling frequency was 128 Hz. After the tests, the well-known frequency domain decomposition (FDD) technique was applied to estimate the fundamental mode of vibration and the associated damping, as shown in Table 1.

For a better comparison between experimental and numerical results, in Table 1, the D_F index was reported, which is defined as:

$$D_F = |(f_{FEM} - f_{exp})/f_{exp}| \cdot 100 \quad (2)$$

where f_{FEM} is the frequency value obtained from the finite element model, and f_{exp} is the one experimentally observed. The lower is D_F, and the better is the agreement between the compared frequencies.

Table 1. Fundamental frequencies of the chimney, with the corresponding participating masses.

		Frequency Hz		Damping %	Mass %
Mode	**FEM**	**Dynamic Test**	**D_F**	**Dynamic Test**	**Trans.**
1	0.863	0.861	0.23%	4.1	81.44
2	2.900	2.840	2.06%	1.6	14.66

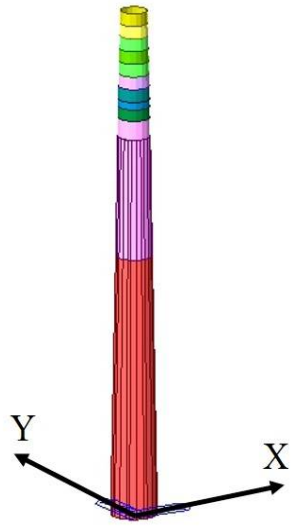

Figure 7. Finite element model (FEM) of the chimney.

The results show that the frequencies, which characterize the first and the second mode, obtained from the FEM, are practically coincident with those evaluated after the dynamic tests performed on the historical masonry chimney. It can be noted that considering the total mass of the chimney equal to m_T = 276,465.40 kg, the modal mass involved in mode 1 is $m_{stru,\ I\ mode}$ = 225,153.29 kg (= 81.4%) [37].

The seismic action is described using a set of seven spectrum-compatible accelerograms [38]. The accelerograms are compatible with the site elastic spectrum prescribed by the code [33] and characterized by the parameters listed in Table 2.

Table 2. Response spectrum parameters.

Life of the Structure V_N	**Year**	**50**
Use category	-	II
Coefficient for use category C_u	-	1
Reference life V_R	year	50
Probability of exceedance P_{VR}	%	10
Topographic coefficient S_T	-	1
Soil category	-	B
PGA	g	0.094

After evaluating the dynamic behavior of the chimney (FEM_1—CASE A), the TMD is introduced in the FEM (FEM_1—CASE B). The TMD is schematized by a nodal mass linked to the chimney by a linear spring-damper element characterized by an equivalent horizontal stiffness (k_{TMD}) and related equivalent damping (c_{TMD}) calculate according to Equations (3a) and (3b) as a function of the mass of the structure involved in the first vibration mode as reported in [39,40]:

$$k_{TMD} = m_{TMD} \cdot \alpha_{opt}^2 \cdot \omega_s^2, \quad (3a)$$

$$c_{TMD} = 2 \cdot \xi_{opt} \cdot (k_{TMD} \cdot m_{TMD})^{0.5}, \quad (3b)$$

where α_{opt} is the optimal coefficient of frequencies, defined as (Equation (4)):

$$\alpha_{opt} = [((1 - 0.5\mu)^{0.5}/(1 + \mu)) + (1 - 2\xi^2)^{0.5} - 1] - [2.375 - 1.034\mu^{0.5} - 0.426\mu] \cdot \xi \cdot \mu - (3.730 - 16.903\mu^{0.5} + 20.496\mu) \cdot \xi^2 \cdot \mu^{0.5}, \quad (4)$$

μ represents the ratio between the TMD mass (m_{TMD}) and the participating mass of the structure involved in the first vibration mode ($m_{stru,\ I\ mode}$), as shown in Equation (5):

$$\mu = m_{TMD}/m_{stru,\ I\ mode}, \quad (5)$$

ξ is the damping ratio of the structure considered, in this case, equal to 0.03. The optimal equivalent viscous damping ratio (ξ_{opt}) is calculated considering Equation (6).

$$\xi_{opt} = [(3\mu)^{0.5}/(8 \cdot (1 + \mu) \cdot (1 - 0.5\mu))] + (0.151\xi - 0.175\xi^2) + (0.163\xi + 4.98\xi^2) \cdot \mu, \quad (6)$$

and ω_s is defined as the pulsation depending on the frequency of the considered vibration mode (in this case, the frequency of the first mode, f_I), defined through Equation (7):

$$\omega_s = 2\pi \cdot f_I, \quad (7)$$

Changing the μ ratio in the range 1–5%, as suggested in [13], a preliminary definition of the TMD parameters is carried out for two different TMD mass positions: (i) at the top of the chimney (40 m height) and (ii) at the top quote of the part of the double skin (about 26.50 m). The optimal μ value (depending upon the values of k_{TMD} and c_{TMD}) significantly reduces the base shear, base moment, and top displacement of the chimney with an acceptable value of the TMD mass [41–43]. Table 3 shows the main TMD parameters considered in this work for the two different positions. It is important to notice that the two proposed TMD configurations are completely independent and designed to work around the first fundamental frequency that characterizes the chimney's dynamic behavior.

Table 3. TMD parameters for the two different positions are considered in this work.

Location m	**M %)**	**m_{TMD} kg**	**k_{TMD} kN/m**	**c_{TMD} kNs/m**
40.00	2.5	5628.83	150.08	5.89
26.50	3.0	6754.60	177.75	7.65

The preferable solution, from a construction point of view, is the one where the TMD is installed at quote 26.50 m, using a connection system with the steel structure (Figure 3b). The main advantage of the 26.50 m height positioning of the TMD is the possibility to avoid reinforcement of the upper part of the chimney, where only one skin is present. Figures 8–10 show the optimization curves, expressed in terms of an average value of base shear, bending moment, and top displacement as a function of μ, obtained by integration of the dynamic equation of the structure under the set of seven spectrum-compatible accelerograms [13,33] considering the TMD positioned at 26.50 m, while Figures 11–13 show the results of the optimization process for the case of the TMD positioned at 40.00 m.

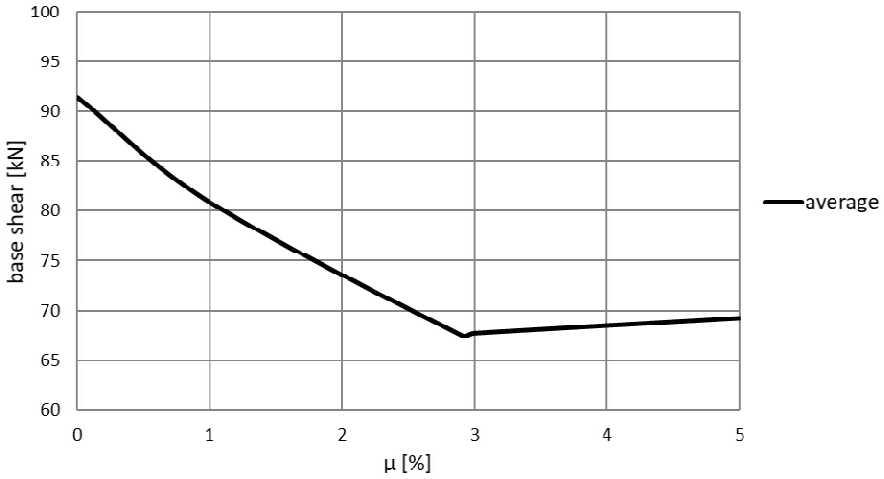

Figure 8. Base shear against the mass ratio, μ considering the TMD positioned at 26.50 m.

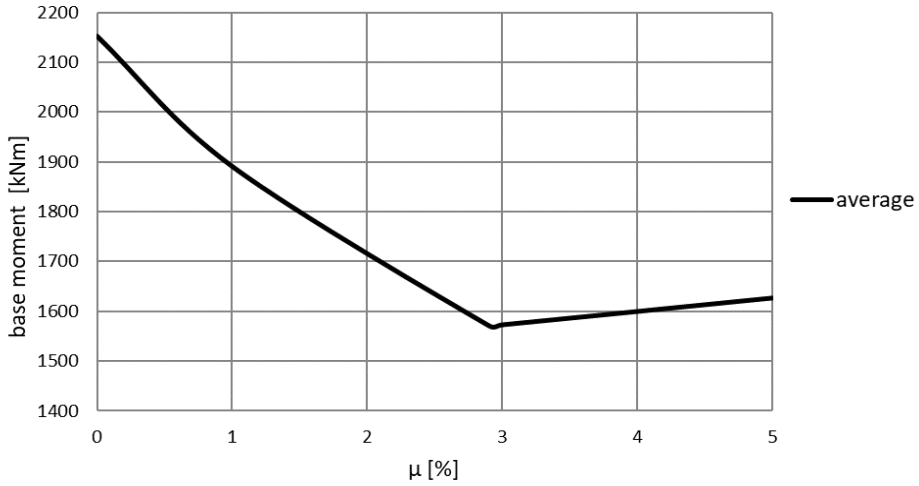

Figure 9. Base moment against the mass ratio, μ considering the TMD positioned at 26.50 m.

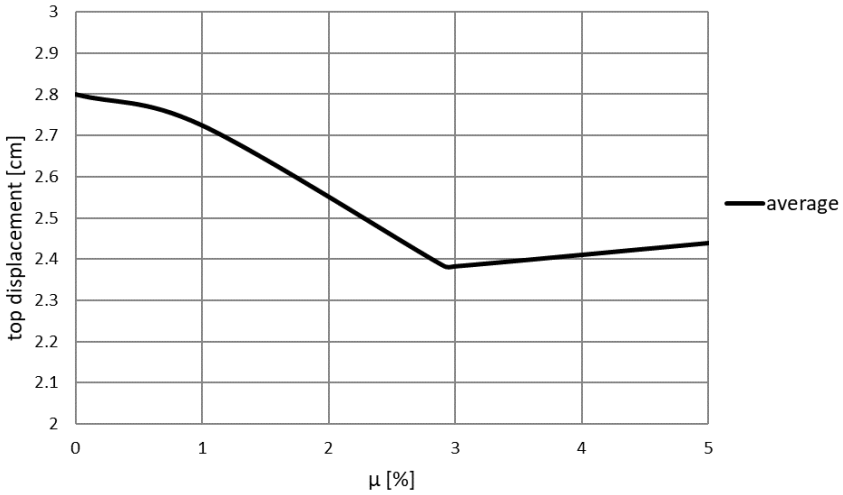

Figure 10. Top displacement against the mass ratio, μ considering the TMD positioned at 26.50 m.

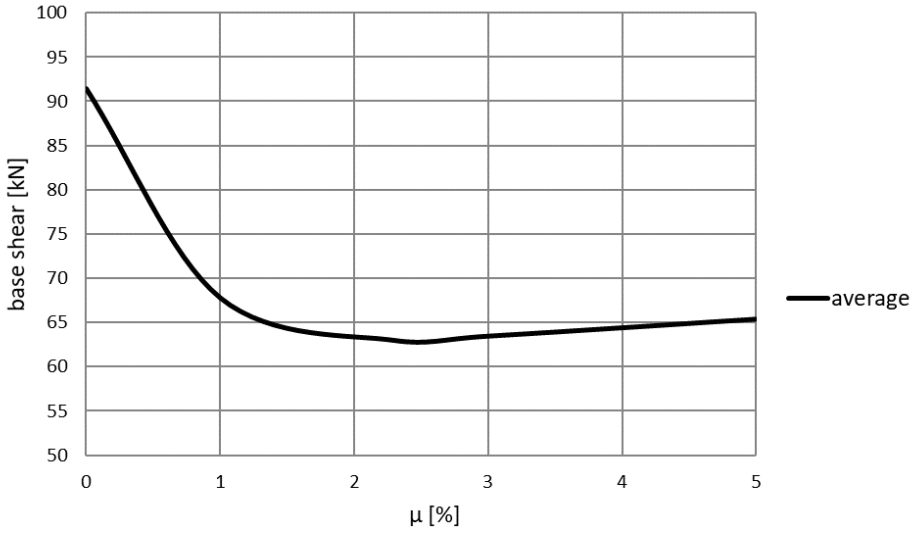

Figure 11. Base shear against the mass ratio, μ considering the TMD positioned at 40.00 m.

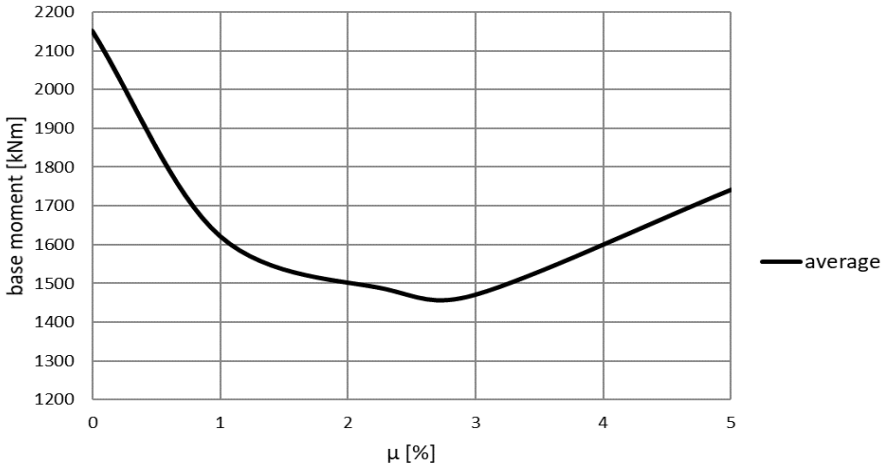

Figure 12. Base moment against the mass ratio, μ considering the TMD positioned at 40.00 m.

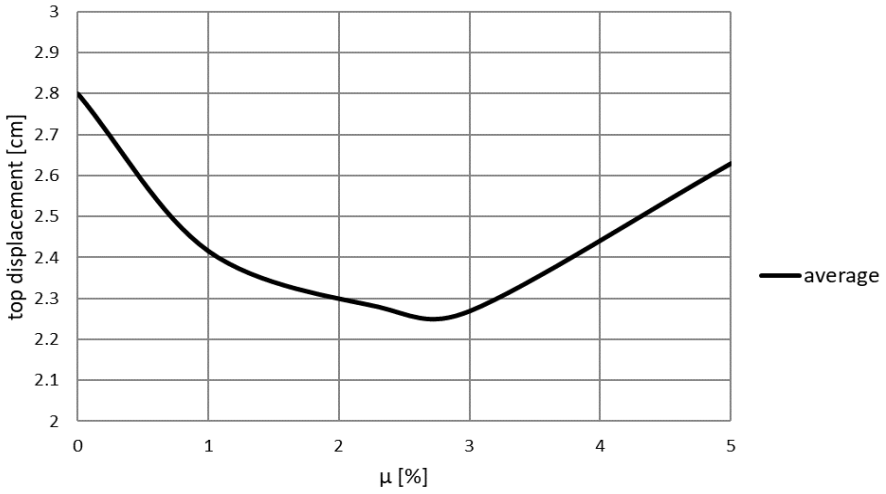

Figure 13. Top displacement against the mass ratio, μ considering the TMD positioned at 40.00 m.

3. Results

From the FEM_1—CASE A, considering the design's seismic action [33,34] and evaluated at the base section of the chimney, it obtained an axial force, F_Z = 2711.20 kN, a bending moment, M_X = 3877.00 kNm, and a shear force, F_y = 151.00 kN. Moreover, the top displacement is equal to 0.060 m is obtained. It is important to highlight that in this case, the maximum compression acting on the chimney base section is equal to 2.35 MPa less than the masonry compressive strength (3.55 MPa). On the contrary, more than half of the base cross-section presents tensile stresses with the neutral axis (n) located at the distance d = 1.60 m from the more compression edge of the section (Figure 14, where G is the gravity center, c is the load application point, n indicates the neutral axis and e is the eccentricity) and consequently several crack patterns can be formed.

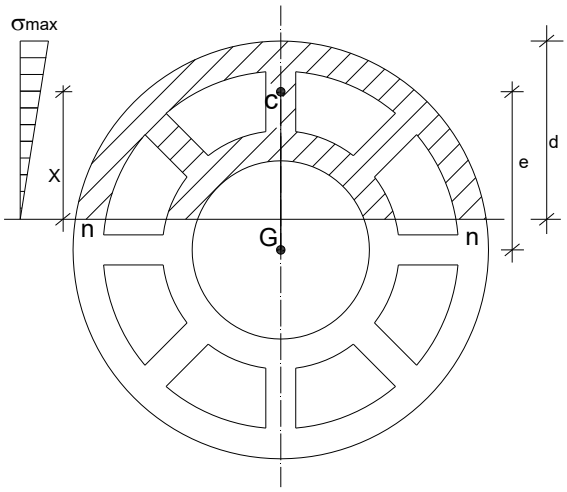

Figure 14. Compressive and tensile stresses distribution on the chimney base cross-section considering the design's seismic action.

Considering that the tensile strength (f_{td}) of the masonry, which characterizes the chimney, is equal to 0, the decompression moment (M_d = 1556 kNm of the base section is calculated through the well-known Equation (8):

$$f_{td} = (F_Z/A_b)/(M_d/W) = 0, \quad (8)$$

where A_b is the area of the chimney base cross-section and W is the section modulus. The obtained value of M_d occurs for a seismic load equal to 41% of the design's seismic action.

Considering the presence of the TMD (FEM_1—CASE B), the values of the actions acting on the chimney base section are F_Z = 2777.44 kN, M_X = 2847.00 kNm, and F_y = 116.70 kN leading to reductions compared to the results obtained for the chimney without the TMD equal to 26.5% for the bending moment and 22.7% for the base shear. Furthermore, the maximum value of the top displacement is equal to 0.042 m (30% lower than the one of FEM_1—CASE A). In this case, the maximum value of the compression stress is equal to 1.86 MPa, significantly lower than the masonry compressive strength and the chimney base cross-section results mostly compressed. In fact, the M_d value is reached for 66% of the design's seismic action. Table 4 summarizes the comparison of the results above discussed considering both the analyzed cases.

Table 4. Comparison of the results obtained from the first linear elastic finite element model (FEM_1)—CASE A and from the FEM_1—CASE B.

Response	Case A	Case B	Δ
base shear kN	151.0.0	116.70	22.7%
base moment kNm	3877.00	2847.00	26.5%

top displacement m	0.060	0.042	30.0%

The presence of the TMD modifies the dynamic behavior of the system. Figure 15 shows the trend of the equivalent damping (ξ_e) as a function of **r** and calculated as indicated in Equation (9):

$$\xi_e = H_{ampl}/2, \quad (9)$$

It can be noticed that the equivalent damping that characterizes the chimney with the TMD is ξ_e = 8.5% obtained considering the average value of the ξ_e calculated in correspondence to the two lower peaks for **r** = 0.95 and **r** = 1.05.

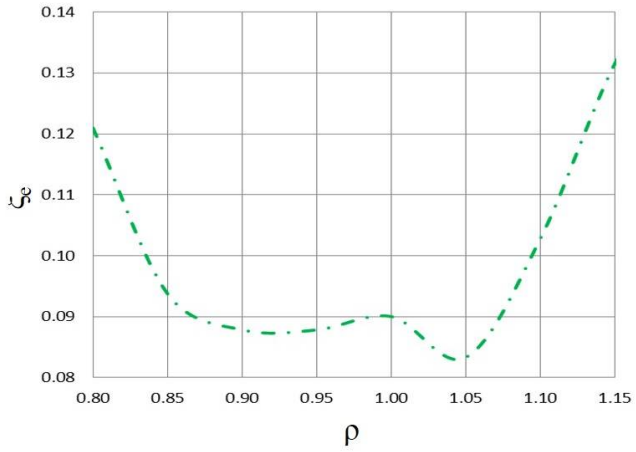

Figure 15. Equivalent damping ratio.

To investigate the TMD functioning over the elastic behavior of the chimney, a fiber model representing the structure without the TMD (FEM_2—CASE A) was implemented to perform pushover analysis [44,45] to obtain the capacity curve of the masonry chimney through the application of a modal load distribution proportional to the first vibration mode. To consider the nonlinear behavior of the masonry, a compression elastic–brittle constitutive law was adopted considering a tensile strength equal to 0. In particular, the chimney's fiber model is divided into beam elements having a height equal to 5 m, to which the nonlinear properties of the masonry are assigned. Figure 16 reports the fiber discretization of the base section.

Figure 17 shows the capacity curve, expressed in terms of base shear and top displacement and where the slope of the green line represents the elastic stiffness of the structure, while the slope of the red line indicates the ultimate secant stiffness before exceeding the compressive strength of the upper edge of the base section (Figure 18) corresponding to the ultimate considered step, $Step_{ult}$.

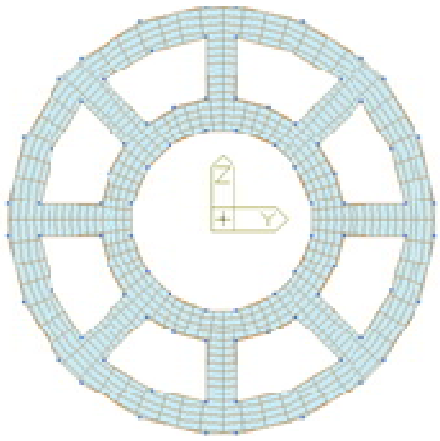

Figure 16. Fiber discretization of the chimney base section.

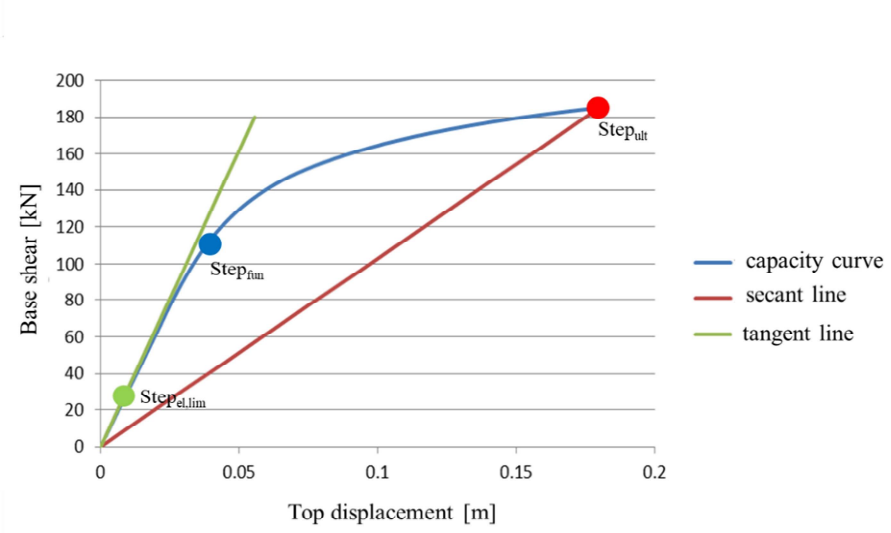

Figure 17. Chimney capacity curve.

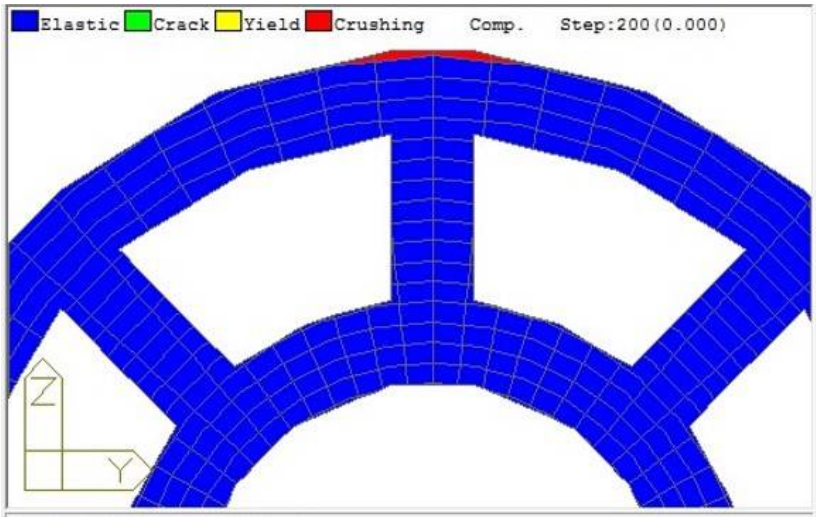

Figure 18. Crushing of the upper edge of the section base due to exceeding the compressive strength.

Considering $Step_{ult}$, the correspondence point on the moment-curvature (M-χ) diagram of each section of the chimney are determined to obtain the scale factor to be

applied to the elastic stiffness of the cross-sections of the chimney calculated as the ratio between the stiffness evaluated in correspondence to the considered point of the capacity curve and the elastic stiffness of the analyzed cross-section. Figure 19 reports the M-χ diagram of the base cross-section.

The scale factor calculated for each section was applied to the corresponding section of the FEM_1—CASE B to perform an eigenvalue analysis. If the TMD is involved in the first two vibration modes, the TMD operating limit ($Step_{fun}$) is obtained. Differently, the process is repeated iteratively considering steps closer to the elastic limit defined by the capacity curve. Table 5 summarizes the ratio between the calculated stiffness obtained in correspondence to the $Step_{fun}$ and the elastic stiffness ($Step_{el,lim}$).

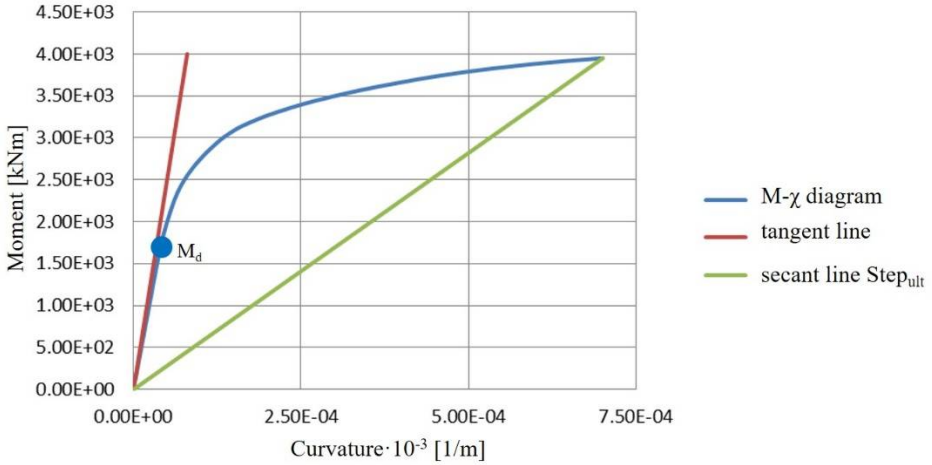

Figure 19. M-χ diagram of the base cross-section.

Table 5. The ratio between the calculated stiffness obtained in correspondence to the $Step_{fun}$ and the elastic stiffness ($Step_{el,lim}$).

Section (m)	Stiffness Ratio (%)
0–5	70%
5–10	78%
10–15	83%
15–20	83%
20–25	89%
25–30	92%
30–35	100%
35–40	100%

4. Discussion

Once the TMD was optimized, and the behavior of the masonry chimney with TMD was investigated considering even the operation of the device over the elastic behavior of the chimney, a standard approach through the execution of nonlinear time-history analysis was executed to confirm the results obtained by the proposed procedure. The seismic action used is represented by Accelerogram 1 of the seven spectrum-compatible accelerograms mentioned in Section 2 (see Figure 20). Figures 21 and 22 show the trend of the top displacement and the base shear of the chimney, with and without TMD, when the structure remains within the elastic range. However, the showed results are valid to the $Step_{fun}$. The optimized TMD benefits are confirmed by significant reductions in the

response obtained both in terms of top displacement and base shear. Consequently, the use of the TMD is an effective solution to reduce the effects of the seismic action. This reveals the TMD capabilities to protect slender historical masonry structures (as the chimney), not only for concrete and/or steel structures. Furthermore, the procedure proposed represents an alternative to the nonlinear time-history analyses, commonly used by the designers to optimize the TMD parameters.

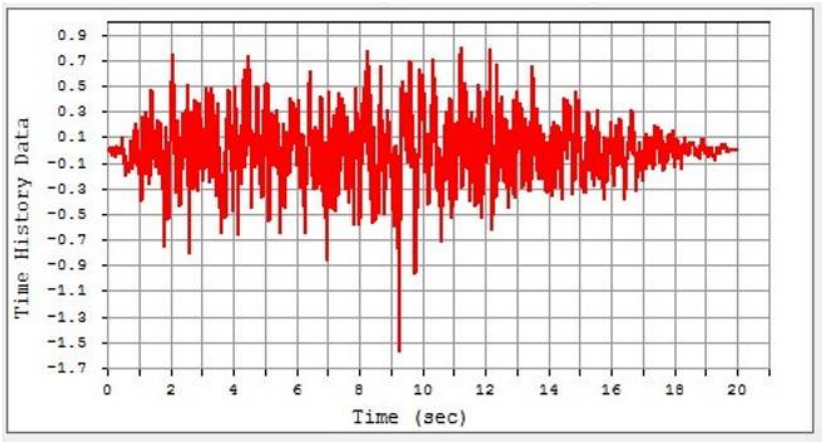

Figure 20. Time history data of acceleration in m/s² (accelerogram 1).

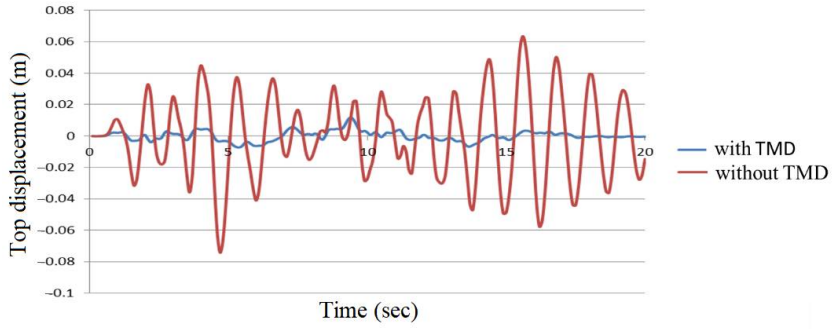

Figure 21. Comparison of the top displacement obtained by the nonlinear time-history analysis when the structure remains within the elastic range.

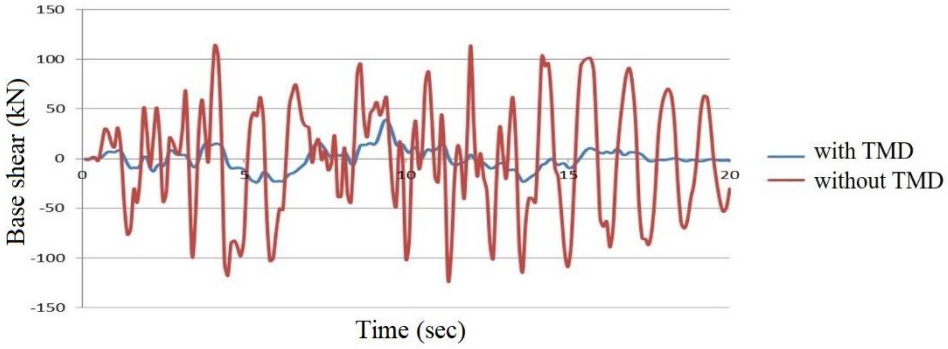

Figure 22. Comparison of the base shear obtained by the nonlinear time-history analysis when the structure remains within the elastic range.

Finally, Figures 23 and 24 show, respectively, the trend of the displacement and the acceleration of the TMD. It is believed that the use of the TMD system to improve the seismic behavior of slender historical masonry structures is vital as it can protect against collapse. The TMD can protect the primary structure against the formation of widespread crack patterns, which can significantly reduce the bending moment acting on the

structure and the resulting decompression effects. Furthermore, the proposed device configurations represent a reversible system that is applicable to structures characterized by a particular historical value.

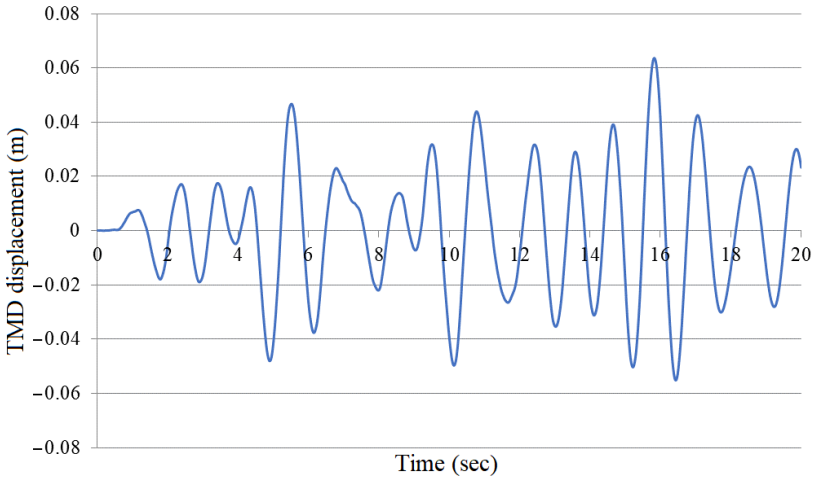

Figure 23. TMD displacement.

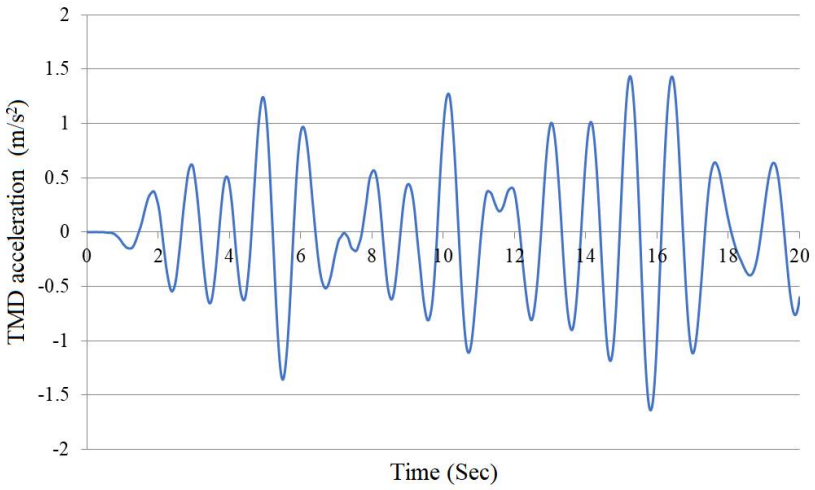

Figure 24. TMD acceleration.

The further development of this study is to apply the proposed procedure to designing TMDs for masonry structures characterized by more complex dynamic behavior.

5. Conclusions

In this paper, an optimization procedure to design TMDs for slender masonry structures was presented. The proposed procedure has two parts: linear and nonlinear analysis. From the linear analysis, the TMD parameters are evaluated for different locations (related to the geometry of the chimney understudy). With the execution of the nonlinear analysis, the TMD's effectiveness over the elastic behavior of the chimney is investigated. In particular, pushover analysis is performed to evaluate the structure's capacity curve and obtain the value of the stiffness reduction for each section of the chimney in correspondence to the different points of the curve. This stiffness reduction is applied to the corresponding section of the linear FEM of the chimney. The comparison between the structural behavior with and without TMD cases is underlined for different stiffness values. The TMD functionality under the seismic action is improved. The

importance of considering a different range of stiffness values is pointed out to improve the TMD functionality over the elastic range of structural behavior. The following improvements, realized under the linear condition, are still valid up to the $Step_{fun}$ of the capacity curve: the top displacement was decreased from 0.060 m to 0.042 m (30%), the base shear was decreased from 151 kN to 116.7 kN (23%), and the base moment was reduced from 3877 kN.m to 2847 kN.m (27%). Over the $Step_{fun}$, the stiffness reductions due to the crack pattern of the masonry contribute to the TMD ineffectiveness. Moreover, the acceleration shown by the TMD system is less than 1 g.

The use of the TMD system to improve the seismic behavior of slender historical masonry structures is vital as it can protect against collapse. The device can also protect the primary structure against the formation of widespread crack patterns, which can significantly reduce the bending moment acting on the structure and the resulting decompression effects. Furthermore, the proposed TMD configurations represent a reversible system that applies to structures characterized by a particular historical value.

Finally, the comparison between the results obtained by the execution of a nonlinear time history analysis confirms the effectiveness of the optimized TMD, designed by the proposed procedure, which can be applied to any type of slender masonry structure.

Author Contributions: Conceptualization, M.Z. and N.L.; software, M.Z. and N.L.; validation, M.Z., N.L., M.S. and A.A.; writing—review and editing, M.Z., N.L., M.S. and A.A. All authors have read and agreed to the published version of the manuscript.

Funding: No external founding have been received for the research.

Institutional Review Board Statement: Not applicable.

Informed Consent Statement: Not applicable.

Conflicts of Interest: The authors declare no conflict of interest.

References

1. Brandonisio, G.; Lucibello, G.; Mele, E.; De Luca, A. Damage and performance evaluation of masonry churches in the 2009 L'Aquila earthquake. *Eng. Fail. Anal.* **2013**, *34*, 693–714, doi:10.1016/j.engfailanal.2013.01.021.
2. Zucca, M.; Crespi, P.G.; Longarini, N.; Scamardo, M.A. The new foundation system of the Basilica di Collemaggio's transept. *Int. J. Mason. Res. Innov.* **2020**, *5*, 67–84.
3. Zucca, M.; Franchi, A.; Crespi, P.G.; Longarini, N.; Ronca, P. The new foundation system for the transept reconstruction of the Basilica di Collemaggio. In Proceedings of the International Masonry Society Conferences, Milan, Italy, 9–11 July 2018.
4. De Matteis, G.; Criber, E.; Brando, G. Damage probability matrices for three-nave masonry churches in Abruzzi after the 2009 L'Aquila earthquake. *Int. J. Archit. Herit.* **2016**, *10*, 120–145.
5. Gattulli, V.; Antonacci, E.; Vestroni, F. Field observations and failure analysis of the Basilica S. Maria di Collemaggio after the 2009 L'Aquila earthquake. *Eng. Fail. Anal.* **2013**, *34*, 715–734, doi:10.1016/j.engfailanal.2013.01.020.
6. Acito, M.; Bocciarelli, M.; Chesi, C.; Milani, G. Collapse of the clock tower in Finale Emilia after the May 2012 Emilia-Romagna earthquake sequence: Numerical insight. *Eng. Struct.* **2014**, *72*, 70–91.
7. Valente, M.; Milani, G. Earthquake-induced damage assessment and partial failure mechanisms of an Italian Medieval castle. *Eng. Fail. Anal.* **2019**, *99*, 292–309, doi:10.1016/j.engfailanal.2019.02.008.
8. Miano, A.; Jalayer, F.; Forte, G.; Santo, A. Vulnerability assessment for masonry buildings based on observed damage from the 2016 Amatrice earthquake. In Proceedings of 7th International Conference on Earthquake Geotechnical Engineering, Rome, Italy, 17–20 June 2019.
9. Jain, A.; Acito, M.; Chesi, C. Seismic sequence of 2016–17: Linear and non-linear interpretation models for evolution of damage in San Francesco church, Amatrice. *Eng. Struct.* **2020**, *211*, 110418.
10. Del Gaudio, G.; Di Domenico, M.; Ricci, P.; Verderame, G.M. Preliminary prediction of damage to residential buildings fol-lowing the 21st August 2017 Ischia earthquake. *Bull. Earthq. Eng.* **2018**, *17*, 4607–4637.
11. Briseghella, B.; DeMartino, C.; Fiore, A.; Nuti, C.; Sulpizio, C.; Vanzi, I.; Lavorato, D.; Fiorentino, G. Preliminary data and field observations of the 21st August 2017 Ischia earthquake. *Bull. Earthq. Eng.* **2019**, *17*, 1221–1256, doi:10.1007/s10518-018-0490-x.
12. Longarini, N.; Crespi, P.G.; Zucca, M. Dissipative cross lam roof structure for seismic restoration of historical churches. In Pro-ceedings of 7th Euro-American Congress on Construction Pathology, Rehabilitation Technology and Heritage Management REHABEND, Caceres, Spain, 15–18 May 2018.
13. Longarini, N.; Zucca, M. A chimney's seismic assessment by a tuned mass damper. *Eng. Struct.* **2014**, *79*, 290–296, doi:10.1016/j.engstruct.2014.05.020.

14. Lagomarsino, S. Damage assessment of churches after L'Aquila earthquake. *Bull. Earthq. Eng.* **2009**, *10*, 73–92.
15. Negro, E.; D'Amato, M.; Cardinale, N. Non-invasive Methods for Energy and Seismic Retrofit in Historical Building in Italy. *Front. Built Environ.* **2018**, *5*, 125, doi:10.3389/fbuil.2019.00125.
16. Turkmen, O.S.; Wijte, S.; De Vries, T.B.; Ingham, J. Out-of-plane behavior of clay brick masonry walls retrofitted with flexible deep mounted CFRP strips. *Eng. Struct.* **2020**, *228*, 111448, doi:10.1016/j.engstruct.2020.111448.
17. Corradi, M.; Sisti, R.; Borri, A. Effect of Thin Cement-Based Renders on the Structural Response of Masonry Wall Panels. *Appl. Sci.* **2018**, *8*, 98, doi:10.3390/app8010098.
18. Jurina, L.; Redaelli, E.O.; Bassoli, A.A. Structural identification through dynamic tests on historic buildings: Some experiences. In Proceedings of IMEKO International Conference on Metrology for Archaeology and Cultural Heritage, MetroArchaeo, Lecce, Italy, 23–25 October 2017.
19. Longarini, N.; Cabras, L.; Zucca, M.; Chapain, S.; Aly, A.M. Structural Improvements for Tall Buildings under Wind Loads: Comparative Study. *Shock. Vib.* **2017**, *2017*, 1–19, doi:10.1155/2017/2031248.
20. Zasso, A.; Aly, A.M.; Rosa, L.; Tomasini, G. Wind induced dynamics of a prismatic slender building with 1:3 rectangular sec-tion. In Proceedings of the VI International Colloquium on Bluff Bodies Aerodynamics Applications, Milan, Italy, 20–24 July 2008.
21. Brownjohn, J.M.W.; Carden, E.P.; Goddard, C.R.; Oudin, G. Real-time performance monitoring of tuned mass damper system for a 183m reinforced concrete chimney. *J. Wind. Eng. Ind. Aerodyn.* **2010**, *98*, 169–179, doi:10.1016/j.jweia.2009.10.013.
22. Ghassempour, M.; Failla, G.; Arena, F. Vibration mitigation in offshore wind turbines via tuned mass damper. *Eng. Struct.* **2019**, *183*, 610–636, doi:10.1016/j.engstruct.2018.12.092.
23. Elias, S.; Masagar, V.; Datta, T.K. Effectiveness of distributed tuned mass dampers for multi-mode control of chimney under earthquakes. *Eng. Struct.* **2016**, *124*, 1–16, doi:10.1016/j.engstruct.2016.06.006.
24. Elias, S. Seismic Energy Assessment of Buildings with Tuned Vibration Absorbers. *Shock. Vib.* **2018**, *2018*, 1–10, doi:10.1155/2018/2051687.
25. Garcia-Diéguez, M.; Koo, K.Y.; Middleton, C.; Brownjohn, J.M.W.; Goddard, C. Model updating for a 183 m of reinforced concrete chimney. In *Dynamics of Civil Structures, Volume 4. Conference Proceedings of the Society for Experimental Mechanics Series*; Proulx T., Ed.; Springer: New York, NY, USA, 2011.
26. Longarini, N.; Zucca, M.; Silvestro, G. The constructions vibration control by tuned mass damper. In Proceedings of IABSE Conference, Geneva 2015: Structural Engineering: Providing Solutions to Global Challenges, Geneva, Switzerland, 23–25 September 2015.
27. Elias, S.; Rupakhety, R.; Olafsson, S. Response control of buildings using TMDI under wind and earthquakes. In Proceeding of 11th International Conference on Structural Dynamics, EURODYN 2020, Athene, Greece, 23–26 November 2020.
28. Li, C. Performance of multiple tuned mass dampers for attenuating undesirable oscillations of structures under the ground acceleration. *Earthq. Eng. Struct. Dyn.* **2000**, *29*, 1405–1421.
29. Wong, K.K. Seismic Energy Dissipation of Inelastic Structures with Tuned Mass Dampers. *J. Eng. Mech.* **2008**, *134*, 163–172, doi:10.1061/(asce)0733-9399(2008)134:2(163).
30. Li, C. Optimum multiple tuned mass dampers for structures under the ground acceleration based on DDMF and ADMF. *Earthq. Eng. Struct. Dyn.* **2002**, *31*, 897–919.
31. Ronca, P.; Crespi, P.; Longarini, N.; Zucca, M.; Zichi, A. Structural analysis for an historical R.C. tall building restoration. In Proceedings of 6th Euro-American Congress on Construction Pathology, Rehabilitation Technology and Heritage Manage-ment, REHABEND, Burgos, Spain, 24–27 May 2016.
32. Simoes, A.; Bento, R.; Gago, A.; Lopes, M. Mechanical characterization of masonry walls with flat-jack tests. *Exp. Tech.* **2016**, *40*, 1163–1178.
33. Ministerial Decree (NTC2018). *Updating of Technical Codes for Constructions (In Italian)*; Official Gazette n°42 of 20/02/2018, Ordinary Supplement n°8; Official Gazette: Rome, Italy, 2018.
34. Ministerial Circular (MC2009). *Instruction for the Application of the New Technical Standards for Buildings. Referred to in the Ministerial Decree of 14 January 2008 (In Italian)*; Official Gazette n. 47 of 26/02/2009, Ordinary Supplement n. 27; Official Gazette: Rome, Italy, 2009.
35. Midas GEN Analysis, www.midasuser.com, accessed in 2021.
36. Saisi, A.; Guidobaldi, M.; Gentile, C. On Site Investigation and Health Monitoring of a Historic Tower in Mantua, Italy. *Appl. Sci.* **2016**, *6*, 173, doi:10.3390/app6060173.
37. Ewins, D.J. *Modal Testing: Theory and Practice*, 2nd ed.; Research Studies Press: Boston, MA, USA, 2000.
38. SISMQKE_GR, Artificial Earthquakes Compatible with Response Spectra, https://gelfi.unibs.it/software/simqke/simqke_gr.htm , accessed in 2018.
39. Rakicevivc, Z.T.; Bogdanovic, A.; Jurukovski, D.; Nawrotzki, P. Effectiveness of tune mass damper in the reduction of the seismic response of the structure. *Bull. Earthq. Eng.* **2012**, *10*, 1049–1073, doi:10.1007/s10518-012-9341-3.
40. Hoang, N.; Fujino, Y.; Warnitchai, P. Optimal tuned mass damper for seismic applications and practical design formulas. *Eng. Struct.* **2008**, *30*, 707–715, doi:10.1016/j.engstruct.2007.05.007.
41. Xie, F.; Aly, A.M. Structural control and vibration issues in wind turbines: A review. *Eng. Struct.* **2020**, *210*, 110087, doi:10.1016/j.engstruct.2019.110087.

42. Chapain, S.; Aly, A.M. Vibration attenuation in high-rise buildings to achieve system-level performance under multiple hazards. *Eng. Struct.* **2019**, *197*, 109352, doi:10.1016/j.engstruct.2019.109352.
43. Aly, A.M. Vibration control of high-rise buildings for wind: A robust passive and active tuned mass damper. *Smart Struct. Syst.* **2014**, *13*, 473–500, doi:10.12989/sss.2014.13.3.473.
44. Bernuzzi, C.; di Gioia, A.; Gabbianelli, G.; Simoncelli, M. Pushover analyses of hand-loaded steel storage shelving racks. *J. Earth. Eng.* **2017**, *21 (8)*, 1256-1282, doi:10.1080/13632469.2016.1210063.
45. Gabbianelli, G.; Kanyilmaz, A.; Bernuzzi, C.; Castiglioni, C.A. A combined experimental-numerical study on unbraced pallet rack under pushover loads. *Ing. Sism.* **2017**, *34 (1)*, 18-38.